Jerez, B., et al. Electro-optic THz dual-comb architecture for high-resolution, absolute spectroscopy, In: *Optics Letters, 44(2), Jan. 2019, Pp. 415-418*

DOI: https://doi.org/10.1364/OL.44.000415

Electro-optic THz dual-comb architecture for high-resolution, absolute spectroscopy

Borja Jerez,* Frederik Walla, Andrés Betancur, Pedro Martín-Mateos, Cristina de Dios, and Pablo Acedo

Electronics Technology Department, Universidad Carlos III de Madrid, Leganés 28911, Spain
**Corresponding author: bjerez@ing.uc3m.es*

An absolute-frequency terahertz (THz) dual-frequency comb spectrometer based on electro-optic modulators for tunable, high-resolution, and real-time rapid acquisition is presented. An optical line of a master frequency comb (filtered via optical injection locking) serves as the seed to electro-optically generate a pair of new frequency combs (probe and local oscillator). Photomixing both combs with another coherent line from the same original master comb generates a narrow linewidth THz dual-comb with teeth frequencies that can be referenced to a radio-frequency standard. The system is validated with a proof-of-principle measurement of a microwave filter in the W-band.

The increasing progress in the terahertz (THz) domain (0.1–10 THz) continues to find new diverse fields of applications such as biology, medical applications, industrial testing, communications, security imaging, and environmental observation [1]. Specifically, THz waves are particularly well suited for gas spectroscopy, offering high discrimination and sensitivity due to the presence of many densely located vibrational and rotational transitions [2]. In the THz region, the use of dual-comb spectroscopy (DCS) [3] presents a great number of advantages that cater to the needs of these applications, namely high spectral resolution, high frequency accuracy, broad bandwidth, and fast acquisition. With this approach, a sample is probed using an optical frequency comb (OFC), thereby inscribing its spectroscopic fingerprint into the discrete comb structure. A second OFC with slightly different mode spacing is used to read out the information. Therefore, when both combs interfere on a detector with adequate bandwidth, the beatnotes between corresponding comb modes give rise to a downconverted comb in the radio-frequency (RF) domain. Thus, the spectral response engraved into this new comb can be processed from this easily accessible low frequency region.

Since the first demonstrations in 2005 [4,5], THz DCS has usually been implemented by a pair of mode-locked lasers with slightly different line spacings: the OFC generated by the first laser is sent through a photoconductive antenna which emitted a THz comb that was then detected with another antenna—or an electro-optic (EO) crystal—driven by the second OFC. Research efforts in this direction have yielded notable results in terms of spectral coverage, frequency accuracy, and resolution [6–8], with recent examples aimed at reducing the complexity associated to these setups [9]. Furthermore, the advent of Fabry–Perot THz quantum-cascade-laser-based frequency combs [10] has also motivated the first demonstrations of THz DCS with these devices [11]. However, this technology is still in its infancy and needs to overcome diverse technical challenges for its widespread adoption [12].

In any respect, frequency combs based on the aforementioned approaches suffer from an inherently weak tuning capability of the frequency comb parameters [13]. Furthermore, as these designs rely on the generation of the two independent combs, elaborate locking schemes or digital post-processing algorithms are commonplace methods to ensure or reconstruct the coherence between OFCs [14,15]. On the other hand, EO dual-combs—generated by the strong modulation of a continuous-wave (CW) laser with a pair of EO modulators (EOMs) [16–20]—represent a compelling alternative that provides flexible control over the line spacing (and, therefore, spectral resolution), adjustable measurement speed, and passively mutual short-term coherence between combs, all in the same easy-to-operate platform. Initially developed in the near-infrared region, their applicability has recently been extended towards the mid-infrared by means of nonlinear conversion mechanisms [21,22]. Clearly, the further maturation of this approach for its deployment into the THz region represents a promising path towards the development of both dual-comb and THz applications.

Here we present an electro-optically synthesized THz dual-comb spectrometer based on photonic THz synthesis of light [23]. The dual-comb scheme and the downconversion process across the frequency domains are illustrated in Fig. 1. Starting from a master EO-OFC in near-infrared, two modes are selected through optical injection locking (OIL) separated f_{THz}, which is an exact multiple of the repetition frequency of the master comb. One of the selected modes acts as a reference tone for the THz generation, whereas the other mode is

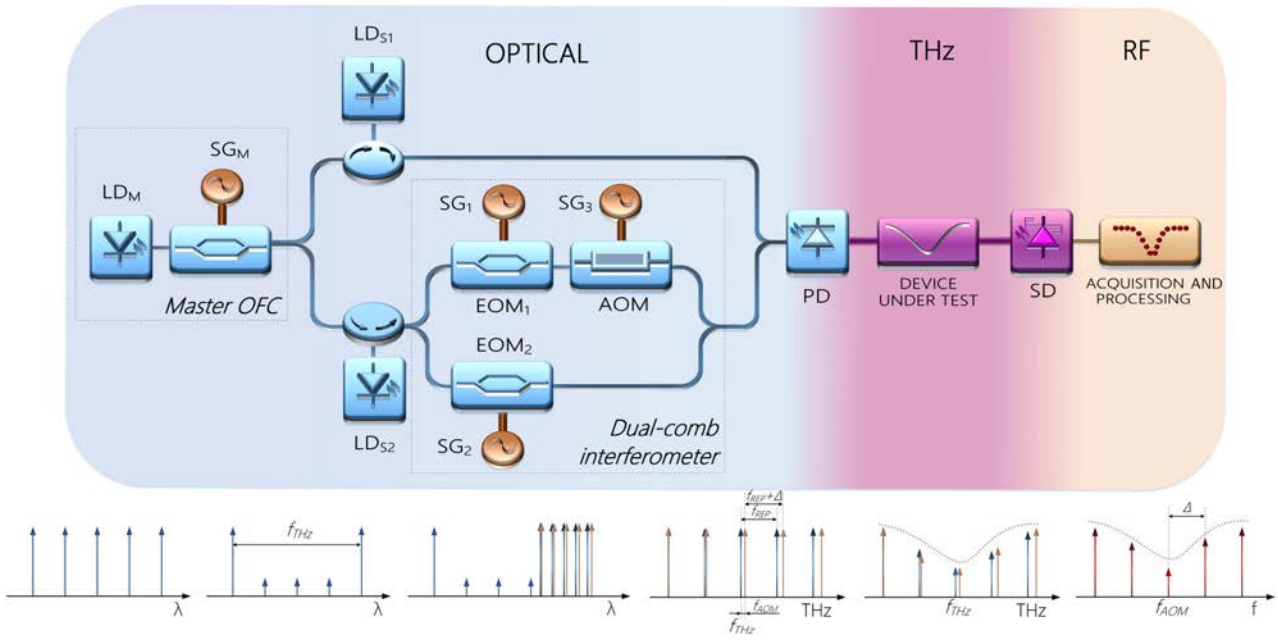

Fig. 1. Experimental setup and sketch of the generation process of the electronically synthesized THz dual-comb. A master OFC serves as a frequency ruler for coherent mode selection via OIL. Phase modulating a first optical mode in two paths generates an optical dual-comb. The signal is photomixed with a second filtered mode from the master OFC to create an ultra-low phase noise THz dual-comb that probes a sample. Overlapping the THz dual-comb in a Schottky diode generates a downconverted comb in the RF domain that can be digitized and processed to obtain the imprinted spectral profile. In alphabetical order, AOM, acousto-optic modulator; EOM, electro-optic modulator; LD M/S, laser diode (master/slave); PD, photodetector; SD, Schottky diode; SG, signal generator.

used as a seed for dual-comb generation. To this end, the latter is split into two paths to be electro-optically modulated at marginally different frequencies (f_{REP} and $f_{\mathrm{REP}} + \Delta$). Additionally, one of these combs is frequency-shifted by an acousto-optic modulator (AOM) f_{AOM} to resolve the symmetric appearance of the dual-comb and ensure the unique mapping of the downconverted combs. Each of the two combs (probe and local oscillator) is then photomixed with the reference tone to create the THz dual-comb. Thus, the central frequency of the THz dual-comb is exactly given by the difference frequency of the two modes previously selected from the master OFC (i.e., f_{THz}), while the line spacing is transferred from the optical domain. The THz dual-comb is then transmitted through a device under test (in this case, a microwave filter) that inscribes its spectral response into the combs. Finally, both THz combs are overlapped in a Schottky diode, triggering a multi-heterodyne process that gives rise to the final RF comb, which exhibits a central frequency defined by the offset frequency between the THz combs (i.e., f_{AOM}) and a line spacing equal to the mismatch between repetition rates (i.e., Δ). The time trace of this downconverted comb can be readily acquired and processed via Fourier transformation or multi-channel lock-in detection [17] to simultaneously reveal the spectral information encoded into each of the teeth of the THz dual-comb. The main parameters of the frequency combs (i.e., their characteristic frequencies) are purely electronically governed by a number of oscillators locked to the same common RF reference, which ultimately fixes the accuracy of the synthesized dual-comb.

The THz EO dual-comb approach, therefore, involves signals which are processed in three different spectral regions. The optical domain section is fully fiberized. First, a discrete mode seed laser (Eblana Photonics, Ltd.) emitting an optical power of ~8 mW at 1542.5 nm is used in conjunction with two cascaded EO phase modulators (EOSpace, Inc.) with a $V_\pi = 3.3$ V in order to produce a master OFC. The same amplified RF signal is used to drive both EOMs with freely selectable frequencies (only limited by the bandwidth of the RF amplifiers and the EOMs). A sample of a representative master comb with a repetition frequency of 18 GHz with a 20 dB span of ~0.95 THz can be seen in Fig. 2.

Using the master OFC as a frequency reference, two of its optical teeth are selected. To that end, the master OFC is split and injected into a pair of DFB slave lasers (QPhotonics, Inc.) with an output power of ~10 mW. Their emission wavelength

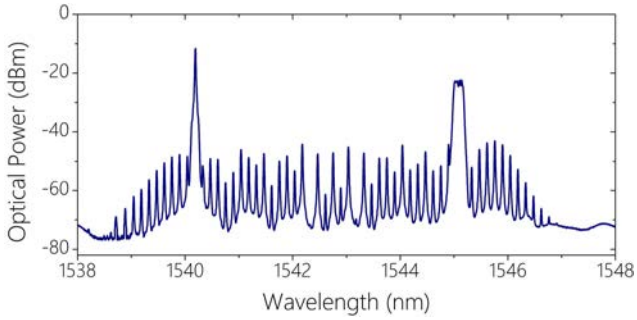

Fig. 2. Optical domain spectrum, including the master OFC and the filtered modes by way of OIL with the slave lasers. In this example, $f_{\mathrm{THz}} = 0.612$ THz. The optical dual-comb is generated from one of the slave lasers (in this case, the red-shifted one) whose lines are not resolved due to the resolution of the optical spectrum analyzer (20 pm).

can be tuned into the proximity of the master comb lines of interest by acting on their current and temperature to conveniently adjust the central dual-comb frequency f_{THz}. The OIL mechanism is further optimized by adjusting the injection ratio (and, hence, the locking range) with variable optical attenuators (not shown in Fig. 1). As mentioned earlier, the light coming from one of the OIL stages is employed as the embryo of an EO dual-comb by dividing its optical power into two paths (as in classic EO dual-combs). Two EOMs (similar to the one taking part in the master OFC) generate a pair of combs with repetition frequencies $f_{\mathrm{REP},1} = 100$ MHz and $f_{\mathrm{REP},2} = f_{\mathrm{REP},1} + \Delta = 100.1$ MHz, with the latter being further shifted in frequency $f_{\mathrm{AOM}} = 40$ MHz with an AOM (Gooch & Housego, Inc.). The resultant optical signal involving the master OFC with both filtered modes and the dual-comb (not resolved) from one of them is depicted in Fig. 2.

The first reference line and the two combs generated out of their counterpart are then recombined and photomixed using a fast photodiode (u2t Photonics, Inc.) with a 3 dB bandwidth in excess of 110 GHz. With 10 mW of input power, a pair of interleaved OFCs is generated in the THz domain with the same line spacings as the optical dual-comb and central frequencies of f_{THz} and $f_{\mathrm{THz}} + f_{\mathrm{AOM}}$, respectively. Figure 3(a) illustrates a pair of interwoven THz combs centered at 96 GHz. Both THz combs are then used to probe the sample in a collinear arrangement before being newly overlapped, this time in a Schottky diode (RPG-Radiometer Physics GmbH) with a bandwidth between 90 and 180 GHz. After RF amplification, this multiheterodyne downconversion reveals the structure of the final RF comb to be analyzed [see Fig. 3(b)], whose central frequency corresponds to the frequency shift induced by the AOM and the line spacing to the mismatch between the repetition frequencies of the combs.

At this point, it is important to remark on some relevant features of the presented system. First, the central frequency of the THz dual-comb (f_{THz}) is exclusively determined by the frequency separation between the pair of slave lasers that filter out the lines of the master OFC, which under perfect locking conditions is simply a multiple of its repetition frequency. As this parameter is adjusted by an external RF signal, its accuracy will be firmly established by the RF standard to which the RF generator is locked. Secondly, the use of a common CW source and the OIL technique, which allows the slave lasers to inherit the phase coherence of the injected source (in this case, the master OFC), as well as a common RF oscillator to generate all the electronic signals, provides the system with an ultra-high degree of mutual coherence. In other words, the potential of this approach hence lies in the fact that all parameters defining the frequencies of each single THz dual-comb mode not only can be arbitrarily chosen, but also directly referenced to an RF standard, which translates into superior capabilities in terms of accuracy and stability.

The performance of the system is assessed with the analysis of the linewidth and the long-term stability of one of the lines of the THz dual-comb. Specifically, the line at 95.9 GHz in the previous example is monitored over a period of 90 min. The results can be seen in Fig. 4(a), where no drift above ± 2.5 Hz is visible. The 3 dB linewidth of the beatnote is below the resolution bandwidth of the spectrum analyzer, a clear indicator of the high mutual coherence of the system. This behavior was observed across all the lines of the narrowband THz comb; however, broader linewidths are expected for higher-frequency THz signals and wider bandwidths due to the scaled phase noise of the RF synthesizer [24]. The frequency stability is also studied through the overlapped Allan deviation [see Fig. 4(b)], showing a type of noise between white FM and flicker FM [25].

Finally, the EO THz dual-comb architecture is validated with the measurement of the transmission spectrum of a

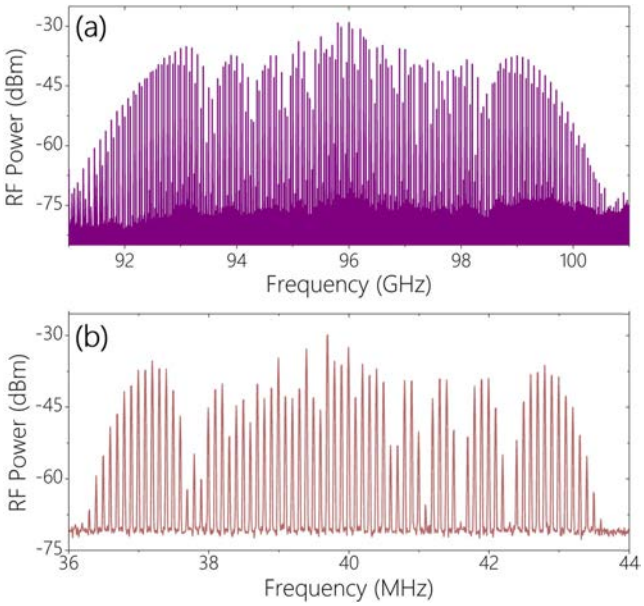

Fig. 3. THz and RF domain spectra. (a) Interleaved THz dual-comb centered at $f_{\mathrm{THz}} = 96$ GHz with $f_{\mathrm{REP},1} = 100$ MHz and $f_{\mathrm{REP},2} = 100.1$ MHz. (b) Downconverted RF comb with a central frequency of $f_{\mathrm{AOM}} = 40$ MHz and line spacing $\Delta = 100$ kHz. The resolution bandwidth of the electrical spectrum analyzers is 10 kHz and 1 kHz in (a) and (b), respectively.

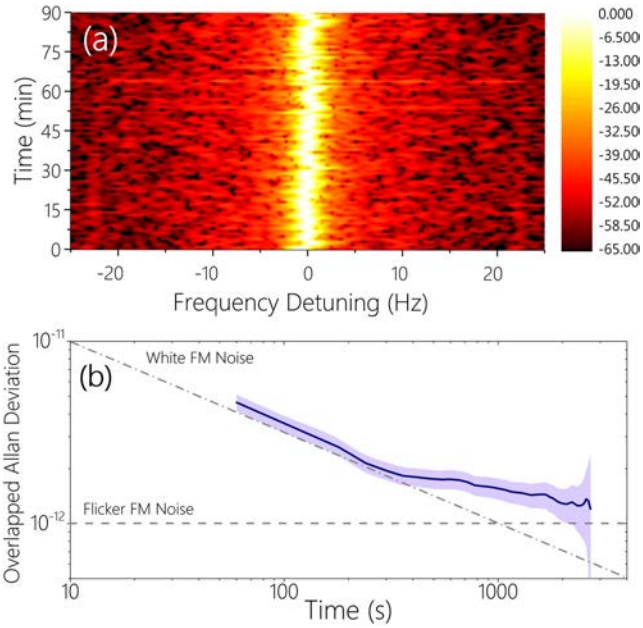

Fig. 4. Evaluation of the performance. (a) Long-term stability analysis of the comb tooth at 95.9 GHz over 90 min in steps of 1 min (the vertical bar on the right indicates the normalized electrical power in dBm). (b) Overlapped Allan deviation (blue trace) of the fractional frequency of the signal at 95.9 GHz and error region (purple trace).

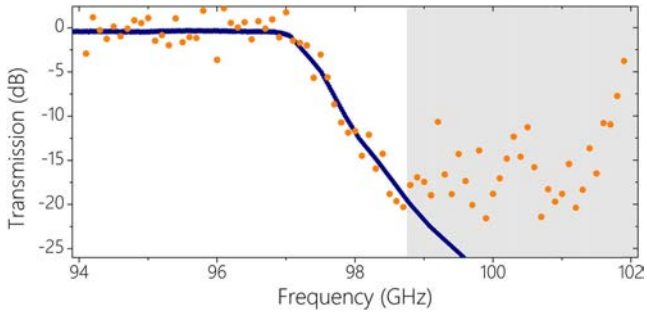

Fig. 5. Transmission spectrum (dots) of the microwave filter when sampled with the THz dual-comb for an integration time of 400 μs. The central frequency of the THz dual-comb is shifted to 98 GHz by the tuning of the electronic settings of the slave lasers and the master OFC. The blue line indicates the frequency response of the filter specified by the manufacturer. The gray shaded area portrays the range of frequencies where the attenuation of the filter is greater than the amplitude of the RF teeth; hence, their dynamic range is insufficient to resolve the spectral information.

microwave filter with cutoff frequency of 97.35 GHz (MI-Wave, Inc.). For that purpose, the time signal (train of interferograms) transmitted by the Schottky diode with a refresh rate of $1/\Delta = 10$ μs is synchronously sampled at 5 GS/s, supplying up to 400 μs of integration time. The Fourier transformation of this signal unveils the structure of the RF comb, from which the spectral information associated to every frequency marker (in this case, the intensity) is obtained. Then each RF mode is directly assigned to its corresponding absolute frequency of the THz comb. Following this procedure, the recovered transmission profile is depicted in Fig. 5 (the signal when no filter is placed in the THz signal path is used as reference for normalization purposes), along with the data provided by the manufacturer. The dots represent the measured response of the filter after coherently averaging 40 interferograms in 400 μs, showing reasonable agreement with the expected profile. The signal-to-noise ratio (SNR) is defined as the ratio of the amplitude of every RF beatnote to its standard deviation when no sample is placed. For the aforementioned integration time, the SNR averaged over all the lines of the RF comb is 102. The normalization of this value for a standard integration time of 1 s and the number of spectral lines ($M = 75$) yields a figure of merit of SNR × M at 1 s of 3.83×10^5 [3].

In summary, we have introduced a new approach for THz dual-comb generation based on EO modulation and photonic synthesis. Owing to the coherent nature of the techniques applied in this system, it is possible to create a THz dual-comb based on a series of ultra-narrow linewidth teeth with a level of accuracy only determined by the RF standard. The method also features the range of virtues associated to EO dual-comb setups, with absolute control over both central and repetition frequencies of the THz combs and measurement speed, as well as very high mutual coherence with the simplicity associated to commercially available off-the-shelf fiber-coupled components. The architecture is successfully validated with the retrieval of the transfer function of a microwave filter in the W-band in a sub-millisecond timescale. The architecture is readily scalable up to the THz region, but the detection arrangement (photodetector and Schottky diode) currently defines the frequency range of the system. In this sense, the incorporation of square-law detectors with a broader bandwidth [26] could quickly extend the capabilities of the system deeper in the THz range and enable further applications such as the analysis of rotational transitions of polar gas molecules.

Funding. Ministerio de Economía y Competitividad (MINECO) (TEC2017-86271-R); Ministerio de Educación, Cultura y Deporte (MECD) FPU Program (FPU014/06338); H2020 European Research Council (ERC) (H2020-MSCA-ITN-2015).

Acknowledgment. B. Jerez acknowledges the support by MECD. F. Walla and A. Betancur acknowledge the support by ERC.

REFERENCES

1. M. Tonouchi, Nat. Photonics **1**, 97 (2007).
2. G. Klatt, R. Gebs, H. Schäfer, M. Nagel, C. Janke, A. Bartels, and T. Dekorsy, IEEE J. Sel. Top. Quantum Electron. **17**, 159 (2011).
3. I. Coddington, N. Newbury, and W. Swann, Optica **3**, 414 (2016).
4. T. Yasui, E. Saneyoshi, and T. Araki, Appl. Phys. Lett. **87**, 061101 (2005).
5. C. Janke, M. Först, M. Nagel, H. Kurz, and A. Bartels, Opt. Lett. **30**, 1405 (2005).
6. G. Klatt, R. Gebs, C. Janke, T. Dekorsy, and A. Bartels, Opt. Express **17**, 22847 (2009).
7. Y.-D. Hsieh, Y. Iyonaga, Y. Sakaguchi, S. Yokoyama, H. Inaba, K. Minoshima, F. Hindle, T. Araki, and T. Yasui, Sci. Rep. **4**, 3816 (2014).
8. T. Yasui, K. Hayashi, R. Ichikawa, H. Cahyadi, Y.-D. Hsieh, Y. Mizutani, H. Yamamoto, T. Iwata, H. Inaba, and K. Minoshima, Opt. Express **23**, 11367 (2015).
9. G. Hu, T. Mizuguchi, R. Oe, K. Nitta, X. Zhao, T. Minamikawa, T. Li, Z. Zheng, and T. Yasui, Sci. Rep. **8**, 11155 (2018).
10. D. Burghoff, T.-Y. Kao, N. Han, C. W. I. Chan, X. Cai, Y. Yang, D. J. Hayton, J.-R. Gao, J. L. Reno, and Q. Hu, Nat. Photonics **8**, 462 (2014).
11. Y. Yang, D. Burghoff, D. J. Hayton, J.-R. Gao, J. L. Reno, and Q. Hu, Optica **3**, 499 (2016).
12. M. Rösch, M. Beck, M. J. Süess, D. Bachmann, K. Unterrainer, J. Faist, and G. Scalari, Nanophotonics **7**, 237 (2018).
13. F. S. Vieira, F. C. Cruz, D. F. Plusquellic, and S. A. Diddams, Opt. Express **24**, 30100 (2016).
14. T. Yasui, R. Ichikawa, Y.-D. Hsieh, K. Hayashi, H. Cahyadi, F. Hindle, Y. Sakaguchi, T. Iwata, Y. Mizutani, H. Yamamoto, K. Minoshima, and H. Inaba, Sci. Rep. **5**, 10786 (2015).
15. D. Burghoff, Y. Yang, and Q. Hu, Sci. Adv. **2**, e1601227 (2016).
16. D. A. Long, A. J. Fleisher, K. O. Douglass, S. E. Maxwell, K. Bielska, J. T. Hodges, and D. F. Plusquellic, Opt. Lett. **39**, 2688 (2014).
17. P. Martín-Mateos, B. Jerez, and P. Acedo, Opt. Express **23**, 21149 (2015).
18. V. Durán, S. Tainta, and V. Torres-Company, Opt. Express **23**, 30557 (2015).
19. A. J. Fleisher, D. A. Long, Z. D. Reed, J. T. Hodges, and D. F. Plusquellic, Opt. Express **24**, 10424 (2016).
20. G. Millot, S. Pitois, M. Yan, T. Hovhannisyan, A. Bendahmane, T. W. Hänsch, and N. Picqué, Nat. Photonics **10**, 27 (2016).
21. M. Yan, P.-L. Luo, K. Iwakuni, G. Millot, T. W. Hänsch, and N. Picqué, Light Sci. Appl. **6**, e17076 (2017).
22. B. Jerez, P. Martín-Mateos, F. Walla, C. de Dios, and P. Acedo, ACS Photonics **5**, 2348 (2018).
23. A. R. Criado, C. de Dios, E. Prior, G. H. Döhler, S. Preu, S. Malzer, H. Lu, A. C. Gossard, and P. Acedo, IEEE Trans. Terahertz Sci. Technol. **3**, 461 (2013).
24. L. Ponnampalam, M. Fice, H. Shams, C. Renaud, and A. Seeds, Opt. Lett. **43**, 2507 (2018).
25. W. J. Riley, *Handbook of Frequency Stability Analysis* (NIST Special Publication, 2008).
26. T. Ishibashi, Y. Muramoto, T. Yoshimatsu, and H. Ito, IEEE J. Sel. Top. Quantum Electron. **20**, 3804210 (2014).